14th International Symposium on Turbulence and Shear Flow Phenomena (TSFP14)
Heidelberg, Germany, July 28-31, 2026

# COLLISION DYNAMICS AND AGGLOMERATION OF ELLIPSOIDAL PARTICLES IN SHEAR FLOW USING THE IMMERSED BOUNDARY METHOD

**C.N. Nolan**
EPSRC Centre for Doctoral Training in Future Fluid Dynamics, University of Leeds, Leeds LS2 9JT, UK
mm18cn@leeds.ac.uk

**J.P. Anderson**
EPSRC Centre for Doctoral Training in Fluid Dynamics, University of Leeds, Leeds LS2 9JT, UK
scjpa@leeds.ac.uk

**L.F. Mortimer**
School of Chemical and Process Engineering, University of Leeds, Leeds LS2 9JT, UK
l.f.mortimer@leeds.ac.uk

**P.K. Jimack**
School of Computer Science, University of Leeds, Leeds LS2 9JT, UK
p.k.jimack@leeds.ac.uk

**M. Fairweather**
School of Chemical and Process Engineering, University of Leeds. Leeds LS2 9JT, UK
m.fairweather@leeds.ac.uk

## ABSTRACT

Particle-particle interactions in shear flows are important in many industrial settings. In the management of nuclear waste, particle-laden sludge must be transported through pipes to long-term storage facilities. During transportation particles experience both turbulent and sheared environments that can lead to a wide range of phenomena such as agglomeration, deposition, flow restriction and clogging. These effects are influenced by the particle morphology which in many cases is highly non-spherical and difficult to study experimentally. This work investigates how particle shape influences collision dynamics and agglomeration under various intensities of shear using fully resolved high-fidelity simulations.

Direct numerical simulations of planar Couette flow using the spectral element solver Nek5000 are conducted. The carrier phase is coupled to the solid phase using a second-order immersed boundary method to fully resolve non-spherical particle-fluid interactions. Spheroidal particles with disk-like (oblate) and needle-like (prolate) morphologies of aspect ratio 5:1 are simulated. Short range interactions are captured using the DLVO interaction model adapted for local surface curvature. Inter-particle collisions are resolved using a hard-sphere framework. A total of 99 binary collision events per morphology are analysed, spanning a range of relative velocities, orientations, and shear rates derived from turbulent channel flow simulations.

Results show that particle morphology influences collision outcomes. Needles exhibit slightly higher agglomeration rates (44%) than disks (40%) and generally attain, and agglomerate under higher relative velocities. Disks generate stronger van der Waals forces due to larger contact areas during collision. The reason the two morphologies fail to agglomerate differs; the needle-like particles often fail to produce sufficient adhesive forces due to in small contact areas resulting from alignment. Disk-like particles get separated by shear forces acting on their large projected areas which overcomes the larger van der Waals attained. These findings highlight the role of particle shape in governing agglomeration dynamics and provide a basis for improving predictive models of particle transport in complex multiphase systems.

## INTRODUCTION

Suspensions of non-spherical particles in turbulent and shear flows are of broad relevance to many industrial processes such as nuclear waste reprocessing, pharmaceutical and minerals processing, as well as sediment transport. In such systems suspended particles are subject to complex orientation-dependent hydrodynamic forces and torques that govern both translational and rotational motion. The collision and potential agglomeration of particles become non-negligible at sufficiently high particle volume fractions and can pose challenges to industry, leading to phenomena such as particle deposition, flow restriction and clogging. Understanding these processes is essential for predicting bulk flow behaviour and informing process design.

The simulation of particle-laden flows has a long history, with much of the foundational work focussing on spherical particles in canonical geometries such as turbulent channel flow (Soldati and Marchioli, 2009; Balachandar and Eaton, 2010). These studies have established well-known phenomena such as turbophoresis (Marchioli et al., 2008) and preferential concentration (Eaton and Fessler, 1994). However, real industrial particles are rarely spherical, and the dynamics of non-spherical particles differ substantially. Later work noted that such particles exhibit orientation-dependent drag, lift and torque with complex coupling between translation and rotation that spherical models cannot capture.

Incorporating particle non-sphericity into numerical simulations poses significant challenges. Point particle approaches such as Lagrangian particle tracking (LPT) apply analytical force and torque expressions derived for isolated ellipsoids in Stokes flow (Marchioli et al., 2010), or leverage orientation dependent projected area-based force formulations (Njobuenwu and Fairweather, 2016) offering computational efficiency at the cost of resolved particle geometry. The immersed boundary method (IBM) offers a high-fidelity, all be it computationally expensive, alternative. In IBM the surface of the particle is fully resolved and represented directly on the fluid mesh (Peskin, 2002; Uhlmann, 2005). This resolves the flow around each particle and enables accurate computation of contact forces during collisions, making the method particularly well suited to four-way coupled regimes where interparticle interactions are important.

Collision and agglomeration modelling for non-spherical particles remains an open challenge. Most existing frameworks rely on simplified spherical contact models or single timestep energy-based agglomeration criteria (Breuer and Almohammed, 2015; Mortimer et al., 2020). These do not capture the time-dependent dynamics of the agglomeration process or the morphology of the resulting aggregates. For non-spherical particles the aggregate shape will influence subsequent dynamics, and resolving this is important both for scientific understanding and for informing lower-fidelity models. In point particle models, attempts have been made to accurately detect the collision between non-spherical particles by representing the particles as a collection of overlapping fictitious spheres (van Wachem et al., 2015) which may be used to resolve the collision using a hard or soft sphere approach.

The physical mechanism driving the agglomeration is governed by the balance between attractive van der Waals forces and repulsive electric double layer forces, described by DLVO theory (Derjaguin and Landau, 1941; Verwey and Overbeek, 1955). Extensions of this framework to non-spherical geometries via local surface curvature (Everaers and Ejtehadi, 2003; Schiller et al., 2011) provide the theoretical basis for agglomeration modelling in the present work.

The present study applies the immersed boundary framework to investigate the dynamics of collision and agglomeration of ellipsoidal particles in shear flows representative of conditions seen in turbulent channel flows. The impact of morphology is investigated by varying particle shape, with fixed aspect ratio, from oblate disk-like particles to prolate needle-like particles. Each species is tracked through the carrier flow with four-way coupling capturing both hydrodynamic feedback and inter-particle collisions. The non-spherical hard-sphere collision algorithm of Jain et al. (2022) is adopted and extended to include DLVO agglomeration forces adapted for ellipsoidal surface curvature. The aim is to characterise how particle morphology influences collision frequency, collision dynamics, and agglomerate formation in various strengths of shear, providing fundamental insight relevant to the nuclear waste processing context where, for example, challenges exist in the transportation of legacy nuclear waste materials from historic storage ponds and silos to interim locations where they are to be safely stored (Mortimer et al., 2020).

## METHODOLOGY

### Fluid-Phase

The solution of the fluid phase is computed through direct numerical simulation of the incompressible Navier-Stokes equations using the spectral element method. In this work the open-source flow solver Nek5000 (Fischer et al., 2008) is used, chosen for its scalability which facilitates parallel computations. The computational domain is a small 0.75 mm cube comprised of 2160 (12×12×15) elements. Each element uses seventh-order Lagrange interpolants on Gauss-Lobatto-Legendre nodes, giving approximately 0.75 million equivalent grid points. This provides high accuracy and sufficient resolution for proper use of the IBM framework. The form of the solved Navier-Stokes equations is:

$$\frac{\partial \boldsymbol{u}}{\partial t} + \boldsymbol{u} \cdot \nabla \boldsymbol{u} = -\frac{1}{\rho}\nabla p + \nu \nabla \cdot [(\nabla \boldsymbol{u} + \nabla \boldsymbol{u}^T)] \qquad (1)$$

$$\nabla \cdot \boldsymbol{u} = 0 \qquad (2)$$

where $\boldsymbol{u}$, $p$, $\rho$ and $\nu$ are the fluid velocity vector, pressure, density and kinematic viscosity, respectively. To impose a constant shear flow in a three-dimensional domain, a planar Couette flow configuration is considered. The cubic domain has periodic conditions in the streamwise ($x$) and spanwise ($y$) directions with no-slip moving walls in the wall-normal ($z$) direction. The walls are given equal and opposite velocities of the form $\boldsymbol{u} = (U_{\dot{\gamma}}, 0, 0)$ where $U_{\dot{\gamma}}$ is the magnitude of the velocity required to achieve a specified constant shear rate $\dot{\gamma}$ thoughout the domain, which is given by:

$$U_{\dot{\gamma}} = \frac{1}{2}\dot{\gamma}H \qquad (3)$$

where $H = 0.75$ mm is the distance between the two walls. A simulation output showing a slice of the domain and constant shear flow field can be seen in Figure 1.

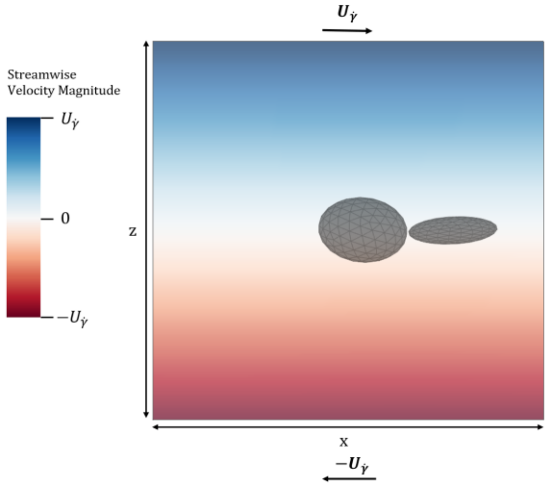


Figure 1: Simulation of fully resolved disks colliding in constant shear flow representative of the bulk flow of a $Re_\tau = 300$ tubulent channel.

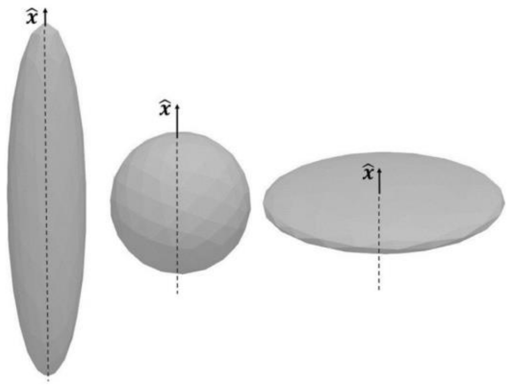


Figure 2: Icospherical particle meshes of a needle, sphere and disk. Symmetry axis unit vectors are shown.

### Particle Morphology

Non-spherical morphologies are modelled using icospherical meshes with 320 triangular faces, scaled along the principal $x$-axis to create prolate (needle) and oblate (disk) spheroids with a constant 5:1 aspect ratio (see Figure 2). By maintaining a constant volume-equivalent spherical radius of 50μm, the characteristic length remains consistent across all geometries. These spheroids exhibit circular symmetry about the *x*-axis, while geometric anisotropy in the *y*- and *z*-directions in the non-spherical cases, introduces orientational dependencies in interparticle force calculations. To ensure high numerical stability and accuracy in tracking these orientational states, the framework employs a quaternion-based approach for the rotation of particle meshes.

### The Immersed Boundary Method

The coupling between the solid phase and the carrier phase is achieved via the use of an immersed boundary method following the method outlined by (Mark and van Wachem, 2008; Anderson et al., 2025). The no-slip condition at a particle's surface is enforced via a ghost-cell mirroring technique, where fluid nodes inside the particle are set to satisfy the boundary condition:

$$\boldsymbol{u}_G = 2\boldsymbol{u}_{IB} - \boldsymbol{u}_E \tag{4}$$

where $\boldsymbol{u}_G$ is the fluid velocity of the ghost node, $\boldsymbol{u}_{IB}$ is the fluid velocity at the surface of the immersed boundary and $\boldsymbol{u}_E$ is the fluid velocity at the exterior point. Interior nodes inside the particle boundary that are not adjacent to the surface are assigned the velocity of the nearest boundary point.

Particle translation and rotation are governed by hydrodynamic forces ($\boldsymbol{F}$) and torques ($\boldsymbol{T}$) computed directly from the fluid pressure ($p$) and viscous stress tensor ($\boldsymbol{\tau}$) interpolated onto the icospherical particle surface mesh. The total force and torque are evaluated numerically as surface sums over all N=320 faces:

$$\boldsymbol{F} = \sum_{i=1}^{N} (-p_i \boldsymbol{n}_i A_i + \boldsymbol{\tau} \cdot \boldsymbol{n}_i A_i) \tag{5}$$

$$T = \sum_{i=1}^{N} \boldsymbol{r}_i \times \boldsymbol{F}_i \tag{6}$$

where the subscript $i$ represents a quantity evaluated at a given face, $\boldsymbol{n}$ is the face unit normal and $A_i$ is the area of face $i$.

The torque is then used to update the angular velocity of the particle by solving Euler's rotation equations in the particle reference frame:

$$\begin{aligned} I_x \frac{d\omega_x}{dt} &= T_x + \omega_y \omega_z (I_y - I_z) \\ I_y \frac{d\omega_y}{dt} &= T_y + \omega_x \omega_z (I_z - I_x) \\ I_z \frac{d\omega_z}{dt} &= T_z + \omega_x \omega_y (I_x - I_y) \end{aligned} \tag{7}$$

where $\boldsymbol{\omega} = (\omega_x, \omega_y, \omega_z)$ is the particles angular velocity and $\boldsymbol{I}$ is its inertial tensor given generally for an ellipsoid as:

$$\boldsymbol{I} = \begin{bmatrix} I_x & 0 & 0 \\ 0 & I_y & 0 \\ 0 & 0 & I_z \end{bmatrix} = \frac{m}{5} \begin{bmatrix} b^2 + c^2 & 0 & 0 \\ 0 & a^2 + c^2 & 0 \\ 0 & 0 & a^2 + b^2 \end{bmatrix} \tag{8}$$

where $m$ is the particle mass, and $a, b, c$ are semi-minor and semi-major axis lengths of the ellipsoid in the $x, y, z$ directions, respectively.

### DLVO Forces

Agglomeration of particles is driven by DLVO forces combining van der Waals attraction and electric double layer repulsion. Due to their short-range nature, the dominant contribution occurs at the point of closest approach between the two particle surfaces. The force is given by:

$$\boldsymbol{F}_{DLVO} = -\chi_{ij}\eta_{ij} \left( \frac{Ar}{12|\boldsymbol{d}|^2} + \frac{64\pi r n k_B T \Theta^2 e^{-\kappa|\boldsymbol{d}|}}{\kappa} \right) \hat{\boldsymbol{d}} \tag{9}$$

where $\boldsymbol{d}$ is the vector of closest approach, $A$ is the Hamaker constant, $r$ is the radius of the sphere with equivalent volume to the ellipsoid, $n$ is the number density of electrolyte ions, $\Theta$ is the reduced surface potential, $k_B$ is the Boltzmann constant, $T$ is the fluid temperature and $\kappa$ is the inverse Debye length.

The first term in Equation (9) is the Hamaker van der Waals attraction and the second is the electric double layer repulsion. The orientational scaling factor $\chi_{ij}\eta_{ij}$, following Everaers and Ejtehadi (2003), accounts for the local surface curvature and relative orientation at the point of closest approach, effectively deepening the potential well for configurations with greater surface interaction. Uniform surface charge is assumed throughout. A cut-off separation of 5 nm is applied to prevent divergence of the Hamaker expression at zero separation. Forces are evaluated at every timestep and included in the full particle force balance.

### Collision Detection and Resolution

Non-spherical particle collisions are modelled using an adaptation of the common-normal method of Jain et al. (2019), which iteratively identifies surface points on spheroids sharing a common normal corresponding to the minimum separation. This distance is used for collision detection and evaluation of short-range DLVO forces.

A hard-sphere model prevents particle overlap. Collisions are triggered when the separation falls below a dynamic threshold based on the relative velocity at closest approach, enabling accurate resolution of van der Waals interactions without prohibitively small timesteps.

The velocity at the contact point is obtained from rigid-body kinematics:

$$\boldsymbol{u}_c = \boldsymbol{u}_p + \boldsymbol{\omega}_p \times \boldsymbol{r}_c \tag{10}$$

where $\boldsymbol{u}_p$ is the particle's translational velocity, $\boldsymbol{\omega}_p$ is the angular velocity of the particle and $\boldsymbol{r}_c$ is the vector from the particle centre to the contact point. Momentum exchange between particles follows Newton's third law and the Poisson restitution hypothesis to update linear and rotational velocities.

Lubrication forces are neglected since van der Waals forces dominate at the particle separations considered.

Particles are advected by fluid forces, exert reaction forces on the fluid through their boundaries, and interact with each other via collisions and inter-particle forces, resulting in a four-way coupled multiphase system.

## RESULTS AND DISCUSSION

For all simulations conducted in this study the fixed particle phase parameters were chosen to represent calcite which is often used as a nuclear waste simulant due to its similar characteristics to nuclear waste materials (see Table 1). The carrier phase is modelled to be water at a temperature of 20 ℃ (see Table 2).

The results presented focus on binary collisions between oblate (disk-shaped) and prolate (needle-shaped) spheroids with an aspect ratio of 5:1, under conditions representative of bulk flow in a turbulent channel. For each morphology, 99 simulations were conducted, covering a wide range of relative velocities, orientations, and shear rates. Identical parameters were applied across morphologies, enabling a direct comparison of how particle shape influences collision behaviour, including agglomeration.

Table 1. Fixed particle phase parameters representing calcite.

| Parameter | Value | Units |
|---|---|---|
| Particle density, $\rho_p$ | 2710 | $\mathrm{kgm}^{-3}$ |
| Volume-equivalent spherical radius, $r$ | 50 | $\mu$m |
| Restitution coefficient, $e$ | 0.4 | – |
| Hamaker constant, $A$ | 22.3 | zJ |
| Inverse Debye length, $\kappa$ | 328,947,368 | $\mathrm{m}^{-1}$ |
| Surface charge density, $\Theta$ | 0.00037 | $\mathrm{Cm}^{-2}$ |

Table 2. Fixed fluid phase parameters used across simulations.

| Parameter | Value | Units |
|---|---|---|
| Fluid density, $\rho$ | 997 | $\mathrm{kgm}^{-3}$ |
| Kinematic viscosity, $\nu$ | $10^{-6}$ | $\mathrm{m}^2\mathrm{s}^{-1}$ |
| Temperature, $T$ | 293 | K |
| Timestep, $\Delta t$ | $2\times10^{-7}$ | s |

Figures 3 and 4 illustrate the typical temporal evolution of the separation distance for disks during agglomeration and bounce events, respectively. For disks, 40 of 99 collisions (40.4%) resulted in agglomeration, while the remaining 59 resulted in bouncing. Needles exhibited a slightly higher agglomeration rate of 44.4% (44 of 99 collisions), suggesting that particle shape influences collision outcomes, with needle-like morphologies showing a slightly greater tendency to agglomerate under identical flow conditions.

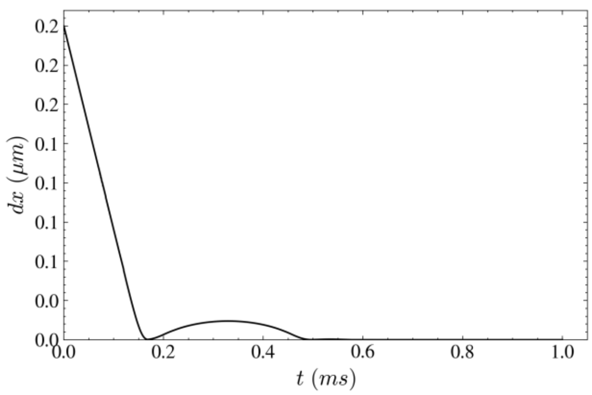


Figure 3: Separation distance over time plot showing the collision and agglomeration of two disks.

The mean separation distance PDFs for needles and disks (Figure 5) reveal distinct behaviours based on particle morphology. Both shapes exhibit a sharp primary peak near zero $dx < 0.1\ \mu$m indicating successful collision and capture due to DLVO forces. The disk agglomeration peak is significantly higher and narrower than that of the needles, suggesting that disks are more effectively drawn into and held at these close proximity ranges. Conversely, bounce events are characterized by a secondary, broader plateau at larger separation distances. While both morphologies show a similar "bounce" distribution between 0.2 and 0.6 $\mu$m, the needles exhibit a more pronounced tail at greater distances, indicating that when separating they do so more quickly, on average.

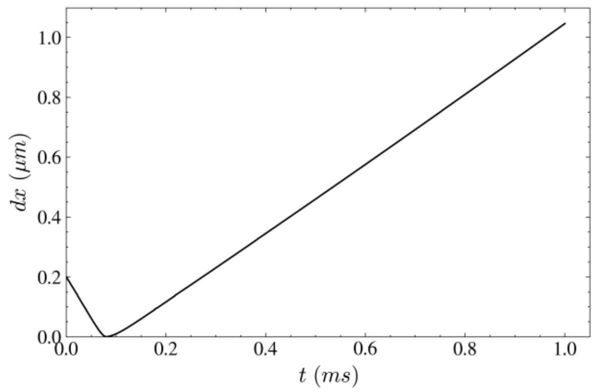


Figure 4: Separation distance over time plots showing the collision and bouncing of two disks.

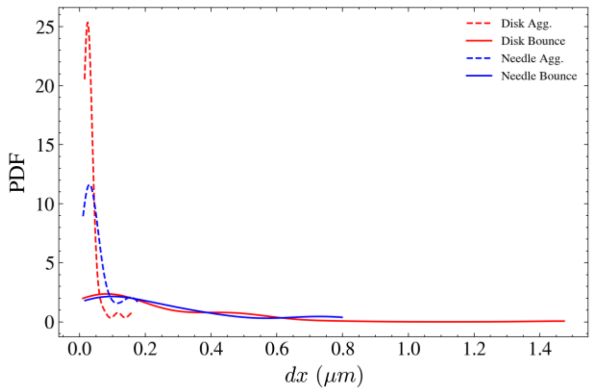


Figure 5: Mean separation distance PDFs, disks (red), needles (blue), agglomeration (dashed), bounced (solid).

The mean relative velocity PDFs are shown in Figure 6 and support this conclusion. We observe higher relative velocities for needle like particles for both agglomeration and bouncing events. For agglomerating disks, we see a sharp peak centred at 0.35 $\mathrm{mms}^{-1}$ which quickly falls off, suggesting that high speed collisions frequently lead to bouncing events. For agglomerating needles, the PDF peaks at a higher velocity (approximately 0.45 $\mathrm{mms}^{-1}$) and maintains a significantly thicker "tail" that extends well beyond 1.0 $\mathrm{mms}^{-1}$. This indicates that needles can successfully stick even during higher-energy impacts. At sufficiently high relative velocities, however, both needles and disks fail to agglomerate as the kinetic energy of the impact overcomes the attractive potential.

The shear rate PDFs (Figure 7) show a similar effect whereby agglomeration seems to be strongly favoured when the shear rate is low, with both morphologies showing a strong peak at $\dot{\gamma} = 0.01$. As the shear rate increases the incidence of bouncing events rises significantly for both shapes. This suggests that elevated fluid energy effectively prevents the formation of an agglomerate, either by inducing high-velocity bypasses that minimise contact time or by providing sufficient hydrodynamic torque to "tear" the particles apart before they can be captured by the DLVO forces.

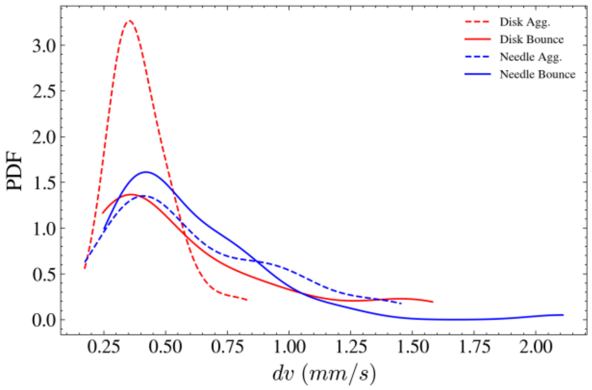


Figure 6: Mean relative velocity PDFs, disks (red), needles (blue), agglomeration (dashed), bounced (solid).

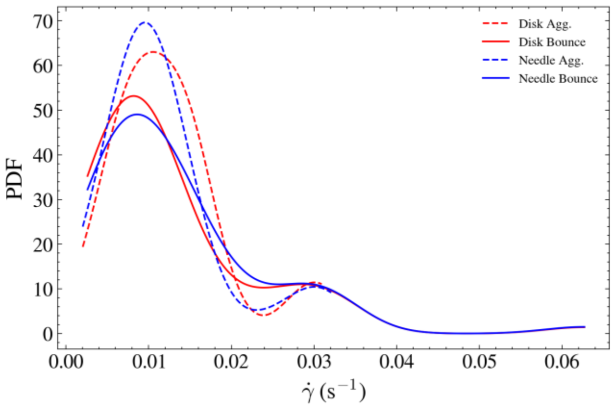


Figure 7: Fluid shear rate PDFs, disks (red), needles (blue), agglomeration (dashed), bounced (solid).

Figure 8 shows PDFs of the maximum van der Waals force magnitude. Disks attain much higher force magnitudes and exhibit greater variance compared to needles. This difference likely arises because van der Waals forces scale with the area of contact between particles. For disks, the broad flat surfaces create larger contact areas during collision, amplifying both the magnitude and variability of the force. Needles, in contrast, have slender geometries that limit the contact area to a smaller, more uniform region, producing lower forces with less variation.

The mean van der Waals force magnitude (Figure 9) reveals that needles and disks fail to agglomerate for fundamentally different physical reasons. For needles the strong bouncing peak at 0 nN indicates that the particles are never within range or their relative orientation is insufficient to produce sufficient attractive forces for agglomeration to occur. The "bounce" distribution for disks reveals a long, flat tail extending up to 17.5 nN. This indicates that for disks, the failure to stick is not due to a lack of force, but rather a lack of time to dissipate momentum. Even when generating these large attractive forces, high-energy collisions provide the particles with enough kinetic energy to overcome the DLVO forces. This allows hydrodynamic shear to pull the surfaces apart before a stable agglomerate can be formed.

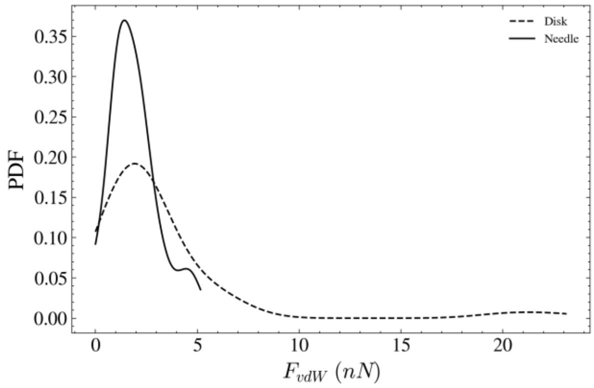


Figure 8: Maximum van der Waals force magnitude PDFs, disks (solid line), needles (dashed line).

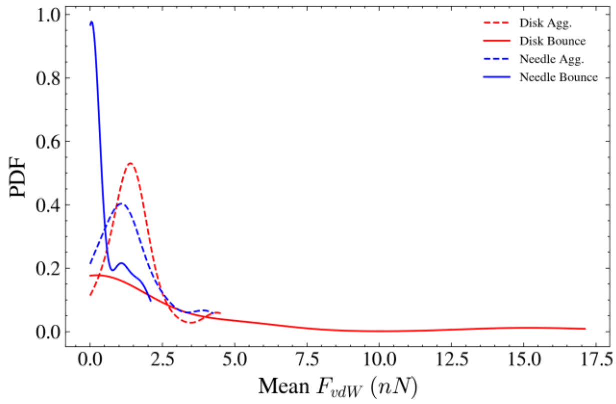


Figure 9: Mean van der Waals force magnitude PDFs, disks (red), needles (blue), agglomeration (dashed), bounced (solid).

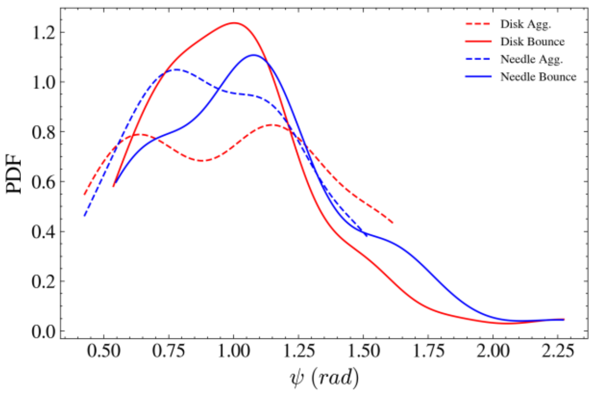


Figure 10: Relative orientation of symmetry axes PDFs, disks (red), needles (blue), agglomeration (dashed), bounced (solid).

PDFs of the relative orientation of symmetry axes are shown in Figure 10. For agglomerating needles, the distribution peaks sharply at 0.75 radians, indicating that they primarily agglomerate when their long axes are angled to allow for maximum surface overlap. When needles approach at more perpendicular angles, the contact area becomes too small to generate an attraction, leading to bouncing events. A similar but less pronounced effect is observed for disk-like particles which exhibit a much broader and more uniform agglomeration profile, suggesting they can successfully engage attractive forces across a wider range of approach angles. The bouncing profiles cover a wide range for both needles and disks, when angles become too large there is not sufficient area to produce strong enough attractive forces for agglomeration. For both disks and needles this angle appears to be between $1.5-1.7$ radians indicating a perfectly perpendicular configuration.

## CONCLUSIONS

Direct numerical simulations of disk- and needle-shaped spheroids under shear show that particle shape influences collision dynamics. While overall agglomeration rates were similar (~40–44%), key morphological differences were observed. The analysis of separation distance and relative velocity PDFs reveals that needle-like particles are capable of successful capture during higher-energy impacts, maintaining a significant agglomeration tail at velocities where disk-shaped particles typically fail.

The investigation into interparticle forces and orientation highlights a fundamental dichotomy in how shape influences capture. For needles, the bottleneck for agglomeration is primarily geometric; the high incidence of zero-force bounce events and the narrow angular window for success near 0.75 rad indicate that needles require precise alignment to generate sufficient attractive potential. Conversely, disks are geometrically more forgiving, engaging significant van der Waals forces across a broad range of orientations. Their primary limitation is kinetic, as their larger contact areas often generate substantial forces that are nonetheless insufficient to dissipate the momentum of high-velocity impacts before hydrodynamic shear pulls the surfaces apart.

These findings suggest that while the net result of collision may appear similar across morphologies, the physical path to agglomeration is not. These results provide a critical foundation for predicting the behaviour of non-spherical particles in complex flows, such as nuclear waste simulants, and suggest that future models must account for the specific interplay between particle geometry and the local shear environment to accurately capture agglomeration dynamics.

## ACKNOWLEDGEMENTS

The authors would like to thank the EPSRC under grant number EP/S022732/1 and Sellafield Ltd for funding.

## REFERENCES

Anderson, J.P., Mortimer, L.F., Hunter, T.N., Peakall, J., and Fairweather, M., 2025, "Numerical Simulation of the Agglomeration Behaviour of Spheroidal Particle Pairs in Chaotic Flows", *Flow, Turbulence and Combustion*, Vol. 114, pp. 941-965.

Balachandar, S., and Eaton, J., 2010, "Turbulent Dispersed Multiphase Flow", *Annual Review of Fluid Mechanics*, Vol. 42, pp. 111-133.

Breuer, M., and Almohammed, N., 2015, "Modeling and Simulation of Particle Agglomeration in Turbulent Flows Using a Hard-Sphere Model with Deterministic Collision Detection and Enhanced Structure Models", *International Journal of Multiphase Flow*, Vol. 73, pp. 171-206.

Derjaguin, B., and Landau, L., 1941, "Theory of the Stability of Strongly Charged Lyophobic Sols and of the Adhesion of Strongly Charged Particles in Solutions of Electrolytes", *Acta Physicochimica*, Vol. 14, pp. 633-662.

Eaton, J., and Fessler, J., 1994, "Preferential Concentration of Particles by Turbulence", *International Journal of Multiphase Flow*, Vol. 20, Supplement 1, pp. 169-209.

Everaers, R., and Ejtehadi, M. R., 2003, "Interaction Potentials for Soft and Hard Ellipsoids", *Physical Review E*, Vol. 67, 041710.

Fischer, P. L., Lottes, J. W., and Kerkemeier, S. G., 2008, "Nek5000", Retrieved 01-08-2022, from http://nek5000.mcs.anl.gov.

Jain, R., Tschisgale, S., and Fröhlich, J., 2019, "A Collision Model for DNS with Ellipsoidal Particles in Viscous Fluid", *International Journal of Multiphase Flow*, Vol. 120, 103087.

Jain, R., Tschisgale, S., and Frohlich, J., 2022, "A Collision Model for DNS with Ellipsoidal Particles in Viscous Fluid [Corrigendum]", *International Journal of Multiphase Flow*, Vol. 150, 104009.

Marchioli, C., Soldati, A., Kuerten, J. G. M., Arcen, B., Taniere, A., Goldensoph, G., Squires, K. D., Cargnelutti, M. F., and Portela, L., 2008, "Statistics of Particle Dispersion in Direct Numerical Simulations of Wall-Bounded Turbulence: Results of an International Collaborative Benchmark Test", *International Journal of Multiphase Flow*, Vol. 34, pp. 879-893.

Marchioli, C., Fantoni, M., and Soldati, A., 2010, "Orientation, Distribution, and Deposition of Elongated, Inertial Fibers in Turbulent Channel Flow", *Physics of Fluids*, Vol. 22, 033301.

Mark, A., and van Wachem, B. G. M., 2008, "Derivation and Validation of a Novel Implicit Second-Order Accurate Immersed Boundary Method", *Journal of Computational Physics*, Vol. 227, pp. 6660-6680.

Mortimer, L. F., Njobuenwu, D. O., and Fairweather, M., 2020, "Agglomeration Dynamics in Liquid-Solid Particle-Laden Turbulent Channel Flows Using an Energy-Based Deterministic Approach", *Physics of Fluids*, Vol. 32, 043301.

Njobuenwu, D. O., and Fairweather, M., 2016, "Simulation of Inertial Fibre Orientation in Turbulent Flow", *Physics of Fluids*, Vol. 28, 063307.

Peskin, C., 2002, "The Immersed Boundary Method", *Acta Numerica*, Vol. 11, pp. 479-517.

Schiller, P., Krüger, S., Wahab, M., and Mögel, H.-J., 2011, "Interactions Between Spheroidal Colloidal Particles", *Langmuir*, Vol. 27, pp. 10429-10437.

Soldati, A., and Marchioli, C., 2009, "Physics and Modelling of Turbulent Particle Deposition and Entrainment: Review of a Systematic Study", *International Journal of Multiphase Flow*, Vol. 35, pp. 827-839.

Uhlmann, M., 2005, "An Immersed Boundary Method with Direct Forcing for the Simulation of Particulate Flows", *Journal of Computational Physics*, Vol. 209, pp. 448-476.

van Wachem, B., Zastawny, M., Zhao, F., and Mallouppas, G., 2015, "Modelling of Gas-Solid Turbulent Channel Flow with Non-Spherical Particles with Large Stokes Numbers", *International Journal of Multiphase Flow*, Vol. 68, pp. 80-92.

Verwey, E.J.W., and Overbeek, J.T.G., 1955, "Theory of the Stability of Lyophobic Colloids", *Journal of Colloid Science*, Vol. 10, pp. 224-225.

Voth, G., and Soldati, A., 2017, "Anisotropic Particles in Turbulence", *Annual Review of Fluid Mechanics*, Vol. 49, pp. 249-279.